Use of a spoof plasmon to optimize the coupling of infrared radiation to Josephson-junction fluxon oscillations

A. Tagliacozzo,[1,2] S. De Nicola,[2] D. Montemurro,[1,2,*] G. Campagnano,[1] C. Petrarca,[3] C. Forestiere,[3] G. Rubinacci,[3] F. Tafuri,[1,2] and G. P. Pepe[1,2]

[1]*Dipartimento di Fisica, Università degli Studi di Napoli Federico II, Via Cintia, I-80126 Napoli, Italy*

[2]*CNR-SPIN, Monte S. Angelo via Cintia, I-80126 Napoli, Italy*

[3]*Department of Electrical Engineering, Università degli Studi di Napoli Federico II, Via Claudio, I-80125, Napoli, Italy*

(Received 12 September 2019; published 8 January 2020)

We show that infrared radiation impinging onto a one-dimensional array of grooves drilled in the superconductor electrode of a long overlap junction can improve matching between fluxon oscillations at THz frequencies and a spoof plasmon of comparable wavelength. This example proves that metamaterials can be very helpful in integrating superconductive and subwavelength optical circuits with optimized matching, bridging the gap between infrared and microwave radiation.

DOI: 10.1103/PhysRevB.101.014506

I. INTRODUCTION

Integrating superconductive and optical circuits in the infrared-microwave frequency range would boost solid state design of quantum information processing in a tremendous way [1–3]. By engineering the optical absorption, single flux quanta in long Josephson junctions can be manipulated [4]. Connecting optical fibers or optical quantum memories [5] with superconducting circuits [6] would increase performances and operating speed as well as reduce power losses [7]. While integrated optics devices usually operate at the single-photon level [8–10], detection of surface plasmon or surface plasmon-polariton (SPP) resonances induced by an evanescent field from a waveguide into a metal film appears as a different promising method to keep the power delivered at the interaction with the solid state device low and controlled [11]. Off-resonance, the evanescent nonpropagating field penetrating into the metal film is reflected back to the photodetector with minimal loss. At resonance, instead, energy is transferred to the metal film generating the surface plasmon mode that can be used to control a superconducting device. At present, detection of surface plasmon or SPP resonances is mostly being developed for biosensors and surface enhanced Raman scattering substrates at visible and near infrared wavelength [12]. Plasmonic photon sorters can be used for spectral and polarimetric imaging [13]. Surface plasmons are already successfully used at very long wavelengths (60–160 μm wavelength) as a guiding solution for THz quantum cascade (QC) lasers [14]. Dielectric-based integrated optics is always limited in scaling by diffraction. Instead, optical generation of plasmon excitations uniquely offers a larger degree of confinement and therefore allows for the creation of structures smaller than the diffraction limit [15,16]. SPPs propagate in metamaterials (MMs) obtained by etching metal surfaces with periodic subwavelength grooves or holes, at infrared frequencies [17–19]. Highly localized plasmon fields can be generated using ordered arrays of nanoparticles or nanohole arrays, instead of thin metal films [20]. Changes in the environmental dielectric will change the plasmon mode and shift the resonance to lower frequencies [21,22].

A large majority of existing MM designs rely on the use of metallic structures sitting on a dielectric substrate [23,24]. However, as the frequency of operation is pushed higher toward the terahertz (THz), infrared, and visible, the Ohmic losses quickly render the current MM approaches impractical. Thus, a top priority is to reduce the absorption losses to levels suitable for device applications. This would require MM designs that do not depend solely on metallic structures and low temperature environment to prevent strong inherent vibrational absorption bands and the high skin-depth losses of the conductors [23,24]. One approach would be to use low power Josephson devices as the MM constituent media which allow dissipationless flow of electrical current [25–28]. Metamaterials with rf SQUID meta-atoms have already been implemented to provide electromagnetically induced transparency (EIT) [29–31].

However, while plasmons belong to the high frequency optical band, Josephson junctions are usually controlled by shaped free space microwaves tones ($\lambda \sim 3$ cm) at a frequency: $\nu = 10^{11}$ Hz, appropriate for fluxon oscillations in long Josephson junctions, which occur at a velocity which is about 1/20th of that of light [32]. This disparity in wave velocities makes it difficult to couple electromagnetic energy in and out of the junction region [33].

In this paper we propose to exploit subwavelength optics to integrate infrared radiation with fluxon oscillations in a long Josephson junction [34]. One of the superconducting electrodes of a long Josephson junction can be modulated in shape, thus inducing periodic variation of the local critical current density which, in turn, is the source of radiative losses in the fluxon dynamics. Infrared radiation impinging

*domenico.montemurro@unina.it

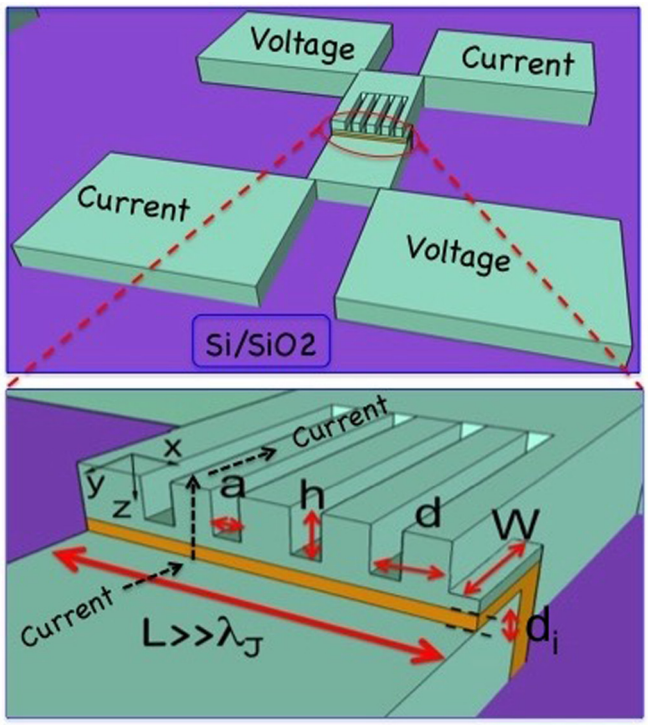

FIG. 1. Layout of the proposed device based on a tunnel Josephson junction. The zooming of the junction shows that the top contact is drilled with a regular array of grooves (in light turquoise) on top of a superconducting sheet (dark turquoise), which is deposited onto the barrier (yellow sheet). The parameters involved are: d, the period of the 1D groove lattice, d_i, the insulating layer thickness (yellow part), and a and h, the distance between the pillars and their height, respectively. W, L, and λ_J represent width, length of the whole array of junctions, and Josephson length, respectively.

on the MM electrode can generate a SPP and appropriate choice of the MM geometry can trigger resonance between fluxon radiation in the insulating junction barrier and the spoof plasmon in the infrared band [35,36]. Such a trick would bridge the gap between infrared and microwave radiation in controlled Josephson systems. The actual realization of the interface between the infrared optical source and the MM, with the desired phase matching conditions for the radiation, is certainly challenging, but it is within present capabilities [37]. However, the matter is not discussed in this paper which is focused on the SPP-fluxon interaction.

It is important to stress that, in the case of application of similar ideas in the quantum information technology, the resulting devices can only take part in the ancillary electronics required to control the qubit array by operating on single fluxon motion, or of the connection between optical memories and the solid state qubit platform, but not directly as coherent devices because they are intrinsically dissipative, although at a very low power level.

In Sec. II we briefly review the theory about how the infrared radiation can generate a SPP in the THz range by irradiating a one-dimensional (1D) subwavelength structure formed by an array of grooves drilled on the top of a normal conductor electrode (see Fig. 1 for a sketch of the structure). We argue that there are limited consequences of the fact that

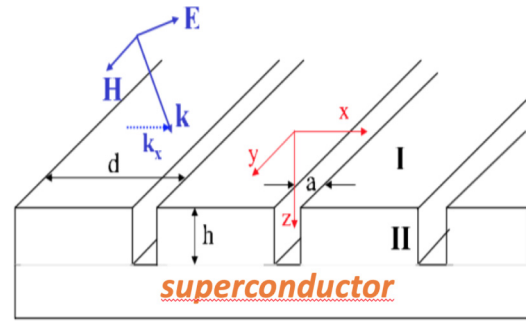

FIG. 2. Sketch of the periodic structure with grooves dug in the topmost electrode of the overlap JJ.

the MM is fabricated in the superconducting electrode of the JJ. In Sec. III we discuss how a fluxon, independently generated in a long overlap Josephson junction, radiates in the junction as a consequence of the periodic modulation of its critical current density. We show that it is possible to design the structure and the active circuit element in such a way that the energy dispersions of the fluxon and of the plasmon cross in the THz range. In Sec. IV we provide a simple model for the interaction between the radiation mode of the fluxon and the SPP mode. The interaction produces an anticrossing of the two mode dispersions and resonant mixture of the two modes provides strong absorption. In Sec. V the motion equation for the fluxon $\varphi(x,t)$ is extended by including the effects due to the presence of the MM modulation and of the SPP interaction. The latter generates a dissipative term which can be recognized as the third order derivative φ_{xxt}, dissipative β term. Additionally, a forcing term arises, which strongly influences the fluxon dynamics, by increasing or decreasing its momentum, according to the phase of the applied perturbation. A simulation of the fluxon dynamics is reported and discussed in Sec. VI in the absence of dissipation. The pendulum motion of the fluxon between the junction edges can be highly perturbed, and the fluxon can be backscattered by a perturbation pulse. Increasing the forcing perturbation, multiple scattered waves are produced which interfere and produce beatings depending on the initial velocity of the fluxon. However, the shape of the principal kink is rather robust with the increase of the perturbation up to some critical velocity. Section VII collects the conclusions. Appendixes A, B, and C report some details on the derivation of the dissipative and forcing terms.

II. SPOOF SURFACE PLASMON DISPERSION

Infrared radiation impinging from vacuum on the surface of a semi-infinite normal metal, on the top of which an array of grooves has been drilled with periodicity $\vec{d} \parallel \hat{x}$, in the $\hat{y}$ direction, of the kind shown in Fig. 2, generates a SPP bound at the surface array and decaying in the inside of the film. Its energy dispersion may saturate in the THz range. The plasma frequency of the SPP dispersion is dictated by the size of the grooves and array geometry. In this section we recall the simplest theoretical derivation of the spoof plasmon bound state generation [18] in an idealized MM structure addressing what are the desired fabrication parameters.

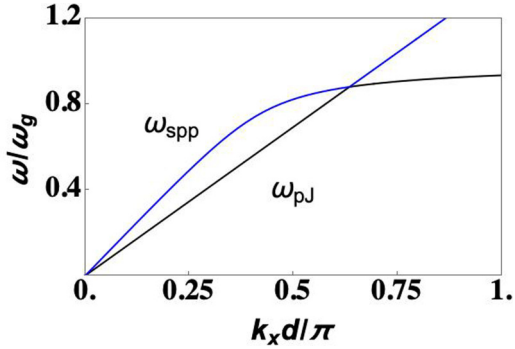

FIG. 3. Dispersion of the spoof plasmon polariton, and of the fluxon radiating energy reported vs k_x on the same plot in unit $(\pi/d, \omega_g = \pi c/2h)$. The parameters used are $d = 0.45$ μm, $h = 13$ μm, $\lambda_J = 100$ μm, $\bar{c} = 0.05c$, and $\omega_J = 1 \times 10^{11}$ s^{-1}.

Let the top surface be at $z = 0$ and the bottom of the grooves be at $z = h$, so that the depth of the grooves is h and their width is a. The TE mode of the field E_x, H_y, propagating in the vacuum, can be expressed as the sum of an incident wave and of reflected waves with reflection coefficients ρ_n, where n is the diffraction order. The subwavelength modulation, which provides diffraction by the periodic structure, is unable to resolve the fine structure, so that the radiation can be averaged in space and continuously matched at $z = 0$. The E_x field is evanescent in $\hat{z}$ $(k_z = i\sqrt{k_x^2 - (\omega/c)^2}$, with $|k_x| > \omega/c)$, but in the limits $\lambda \gg d \gg a$ we can neglect the penetration of E_x into the semi-infinite bulk of the normal metal and impose its vanishing at $z = h$. As the wavelength of the radiation is much larger than the width of the grooves $(\lambda > 2\, n_g\, a$, where n_g is the refraction index inside the groove), just the fundamental mode can be considered in the region $-h < z < 0$. Within these approximations, a very simple relation arises from the matching conditions, which provides the dispersion relation when reflectivity ρ_0 is taken to diverge [18]:

$$\frac{\sqrt{k_x^2 - k_0^2}}{k_0} = S_0^2 \tan(k_0 h), \tag{1}$$

where $\omega = c\, k_0$ and $S_0^2 = a/d$. At large k_x, ω saturates at $\omega_{\rm spp} = c\frac{\pi}{2h}$, as if the groove acted as a cavity waveguide (vacuum is assumed in the grooves). By choosing $d = 0.45$ μm, $h = 13$ μm, and $S_0^2 \sim 0.2$, we find $\omega_{\rm spp} \approx 0.33 \times 10^{14}$ Hz. The plot of the SPP, obtained by solving Eq. (1), is reported in Fig. 3 [18]. The units chosen in the plots for k_x and ω are $(\pi/d, \pi c/2h)$. The additional quasilinear dispersion appearing in Fig. 3 is the radiation field due to the fluxon given by Eq. (8) and discussed in the next section.

III. FLUXON RADIATING IN A MODULATED SUPERCONDUCTING JOSEPHSON JUNCTION

As discussed in the Introduction, an infrared radiation impinging in free space on the top electrode of an overlap JJ of frequency ω couples weakly to the fluxon dynamics due to the mismatch between the radiation wavelength λ and the typical length scale—Josephson length—λ_J of the fluxon. By modulating the top electrode of an overlap JJ in the form of a metamaterial (MM), sketched in Fig. 1, we find that the interaction between radiation coming from the vacuum and the fluxon can be enhanced.

We consider a $S_{\rm MM}/I/S$ long overlap Josephson junction of length $L \parallel \hat{x}$. Here $S_{\rm MM}$ stands for one of the superconducting banks, let us say the top one, in which an array of grooves has been drilled in the $\hat{y}$ direction, as the one sketched in Fig. 2 and presented in Sec. II. S denotes the bottom uniform and homogeneous superconductor electrode, while I stands for insulator of thickness d_i and width w. The SPP device based on the proposed layout (see Fig. 1) could be built using top-down nanofab techniques that include steps of electron beam lithography, dry and wet etching [38–40] for writing, and then drilling the array of junctions, for example, inside a $Nb/NbO_x/Nb$ or $Al/AlO_x/Al$ trilayer sample. We expect that the most relevant effect of the added periodic modulation of the electrode is a corresponding modulation of the Josephson critical current density j_c. The inhomogeneities introduced by the diffractive grating attract or repel the fluxon in its propagation. The dips in the modulation tend to attract and localize the fluxon, while the mesas tend to delocalize it.

The problem was studied long ago both theoretically and experimentally [35] in junctions of millimeter size. They prove that a fluxon shuttling to and from in a periodically inhomogeneous overlap junction radiates. As the derivation of the energy dispersion of the radiating fluxon is based on perturbation of the fluxon propagating in a homogeneous junction, we start here recalling the usual approach to the homogeneous problem.

The gauge invariant form of the supercurrent, written in terms of the phase of the order parameter of the top and bottom electrodes $\vartheta_\pm$ and of the vector potential $\vec{A}$, is

$$\vec{J}^s = -\frac{2e}{2m}|\psi_0|^2\left(\hbar\vec{\nabla}\vartheta + \frac{2e}{c}\vec{A}\right). \tag{2}$$

Here m and $-e$, with $e > 0$, are the electron mass and charge, respectively, and $|\psi_0|^2 = n_s$ is the superfluid density. ϑ is the phase of the superconducting order parameter. The usual approach to the equation of motion for the phase difference $\varphi = \vartheta_+ - \vartheta_-$ in a 1D overlap junction of length L, along the $\hat{x}$ axis, is to consider the z component of the Maxwell equation:

$$\nabla \times B|_z - \frac{\epsilon_r}{c}\frac{\partial E_z}{\partial t} = \frac{4\pi}{c}\left\{J_J - \frac{1}{\lambda_J^2}\frac{V}{R}\right\}, \tag{3}$$

where $J_J = J_c \sin\varphi$ is the Josephson current of critical current J_c, V is the voltage difference across the barrier, and R is the quasiparticle resistance in the insulating layer. The length scale characterizing the spacial variation of φ is the Josephson length λ_J. To be concrete, estimates will be presented for a junction with Nb superconducting contacts with $L \gg \lambda_J$, where λ_J is of the order of various tens of μm. The width d_i of the insulating barrier, along the $\hat{z}$ axis, is of few nanometers.

In the case of bulky superconducting banks one recognizes that the phase difference φ, at points where the superconducting screening currents $\vec{J}^s$ of Eq. (2) have vanished, takes the value dictated by unperturbed superconductors. This allows us to relate the Laplacian of φ to the z component of the curl B

of Eq. (3), obtaining

$$\frac{\partial^2\varphi}{\partial x^2}+\frac{\partial^2\varphi}{\partial y^2}-\frac{1}{\bar{c}^2}\frac{\partial^2\varphi}{\partial t^2}=\frac{1}{\lambda_J^2}\left\{\sin\varphi-\alpha'\frac{\partial\varphi}{\partial t}\right\}, \tag{4}$$

which is the celebrated Sine-Gordon (S-G) equation for the superconducting phase difference at the overlap junction. Here

$$\bar{c}^2=\frac{1}{1+2\lambda_L/d_i}\frac{c^2}{\epsilon_r},\quad \lambda_J^2=\frac{c\phi_o}{8\pi^2 J_c(d_i+2\lambda_L)},$$
$$\omega_J=\frac{\bar{c}}{\lambda_J}=\left(\frac{2\,e}{\hbar}\frac{I_c}{C}\right)^{1/2},\quad \alpha'=\frac{\hbar}{2eRI_c}. \tag{5}$$

λ_L is the London penetration length, $\lambda_L^{-2}=4\pi|\psi_0|^2e^2/(mc^2)$ ($\sim$50 nm for Nb). Dimensionally the Josephson critical current density is $J_c\sim e/(t\mathcal{A})$, where $\mathcal{A}$ is a cross sectional area pierced by the supercurrent J in the $\hat{z}$ direction of the overlap junction and t represents the time. We have estimated a $J_C\sim 100$ A/cm^2 (at temperature of 300 mK) for a device that has $a=d\sim 200$ nm and $w=1$ μm.

The capacitance of the junction, expressed in terms of the thickness of the barrier d_i, $C=\epsilon_r\mathcal{A}/(4\pi\, d_i)$, is rather large, so that charging effects are assumed to be absent. α' is a parameter accounting for the ohmic (zero frequency) dissipation. In the presence of an incoming radiation of wavelength $\lambda\sim 700$ nm, we have $\lambda_J\gg\lambda$.

In the absence of dissipation ($\alpha'=0$), the kink solution for the 1D approximation to Sine-Gordon equation [Eq. (4)] is

$$\varphi_0(x\pm ut)=4\arctan\,\exp\left[\frac{x\pm ut}{\sqrt{1-u^2/\bar{c}^2}}\right], \tag{6}$$

where $u<\bar{c}$ is the velocity of the fluxon.

In the presence of the perturbation induced by the incoming radiation, an additional field $\vec{B}^{(2)}$ will be considered in Sec. V, to be added to the one of Eq. (3). For the time being we consider in this section only the perturbation induced on the fluxon by the groove array at the top contact. We assume that the effect induced by this modulation is to cause a modulation of J_c: $J_c=J_{c0}+J_{c1}\cos\frac{2\pi}{d}x$ in the nondissipative case as follows. If $J_{c1}<J_{c0}$, to lowest order, a solution of the motion equation for the fluxon can be searched by adding a correction to the unperturbed fluxon of Eq. (6), as follows: $\varphi(x,t)=\varphi_0(x,t)+\varphi_1(x,t)$. It has been shown [35,41] that the perturbation $\varphi_1(x,t)$ can take the form of a plane wave:

$$\varphi_1(x,t)=\sum_{n\neq 0}A_n\,\exp\left[i\left(\omega_{\rm pl}t-k_{\rm pl}^n x\right)\right], \tag{7}$$

generating a transverse radiation field $\varphi_t\propto E_z$, $\varphi_x\propto H_y$ corresponding to the plasma frequency $\omega_{pJ}^n/2\pi$ and wave vector k_{pJ}^n given by (here $\nu=\sqrt{1-u^2/\bar{c}^2}$ and n integer)

$$\omega_{pJ}^{n\,2}-\bar{c}^2k_{pJ}^{n\,2}=\omega_J^2, \tag{8}$$

$$\omega_{pJ}^n=\frac{2\pi\,n}{d}\frac{u}{\nu^2}\pm\frac{u}{\lambda_J\nu}\sqrt{\left(\frac{u}{\bar{c}}\frac{2\pi\,\lambda_J\,n}{d\,\nu}\right)^2-1},$$
$$k_{pJ}^n=\frac{2\pi\,n}{d}\frac{u^2}{\bar{c}^2}\frac{1}{\nu^2}\pm\frac{1}{\lambda_J\nu}\sqrt{\left(\frac{u}{\bar{c}}\frac{2\pi\,\lambda_J\,n}{d\,\nu}\right)^2-1}. \tag{9}$$

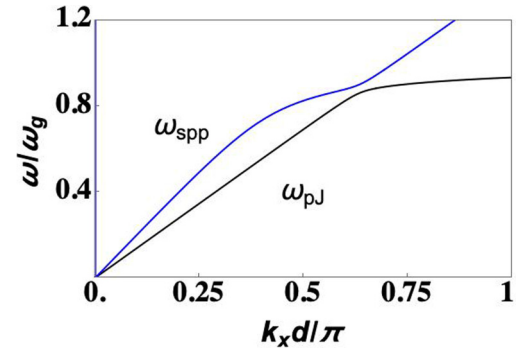

FIG. 4. Anticrossing at the mode interaction vs $k_x\equiv k$. The parameters are the same as in Fig. 3.

The accelerated fluxon radiates in the MM and Eq. (8) is the dispersion law of the radiation. The approximated form is valid for the far field away from the soliton, with emissions ahead of the fluxon (+), or far away behind the fluxon (−). It can be shown that the amplitudes A_n of the plasma oscillations decrease exponentially as n increases, so that we will concentrate only on the term $n=1$. Increasing $u/\bar{c}$, both k_{pJ} and ω_{pJ} increase. An estimate of k_{pJ} for $d=0.45$ μm, $h=13$ μm, $\lambda_J=100$ μm, $\bar{c}=0.05c$, $\omega_J=1\times 10^{11}$ s^{-1}, and $u/\bar{c}\sim 0.8$ gives $k_{pJ}^{n=1}[-]: d/\pi\sim -0.89$. The corresponding radiation frequency is, from Eq. (8), $\omega_{pJ}^{n=1}\sim 0.93\times 10^{14}$ Hz, which is comparable with the plasma frequency of the SPP. These parameters are used in the plot of Fig. 3. Note that ω_J is about three orders of magnitude smaller than ω_{pJ}, so that the dispersion of Eq. (8) is practically linear. The dependence of k_{pJ} on the fluxon velocity is first order in $u/\bar{c}$. In the next section we discuss a simplified model for the interaction between the fluxon radiating field and the SPP originated by the MM, which leads to absorption of energy from the radiation source.

IV. MODES INTERACTION AND ANTICROSSING

As shown in Fig. 3, the SPP dispersion and the radiation mode of the fluxon cross at $k_x\sim 0.6\,\pi/d$ for $d=0.45$ μm and $h=13$ μm. The presence or absence of the crossing strongly depends on the choice of ratio d/h. The fluxon extends over a length λ_J much larger than the period of the modulation in the MM d, so that it is reasonable to assume that it moves at an average velocity prior to interaction with a SPP pulse. The initial velocity should be also determined by accounting for the dissipation mechanisms acting in the dynamics [tuned by the parameters α' appearing in Eq. (4) and β, to be introduced in the following]. These mechanisms also determine the dynamics of the fluxon and, in turn, its radiative power. We address this point in Sec. V and Appendixes A and B. On average, we assume that the fluxon keeps an average stationary velocity during its motion so that we are in the presence of steady state radiation, except when under the action of a short perturbing pulse. This is a very crude approximation, of course, which, however, allows us to modelize the interaction between the SPP and the fluxon radiation mode with a very simple approach. The crossing in Fig. 3 turns into an anticrossing as shown in Fig. 4.

The model rests on a few simplified assumptions. An electric field from the MM in the nondissipative superconductor boundary generates a time derivative of the current density according to the London equation:

$$\frac{\partial}{\partial t}J = \frac{n_s e^2}{m}E, \tag{10}$$

where $n_s e^2/m = c^2/(4\pi\,\lambda_L^2)$. The motion equation (in the $\hat{x}$ direction along the boundary) for the current in time Fourier transform is [$\omega_{pJ} \equiv \omega_{pJ}(k_{pJ})$]

$$-\omega^2\,J + \omega_{pJ}^2\,J = -i\,\omega\,\frac{c^2}{4\pi\,\lambda_L^2}E. \tag{11}$$

This is the first equation relating the current density at the boundary with the insulating barrier and the electric field of the radiating fields.

An additional equation is provided by the relation between the dissipative flow of the added J current and the electric field. In a normal metal, the resistivity $\rho(\omega)$ can be related to the dielectric function $\epsilon(\omega)$ as

$$(-i\,\omega\rho)^{-1} = \epsilon(\omega) - 1. \tag{12}$$

The AC electrodynamics of a superconductor for $\omega < 2\Delta/\hbar$ (Δ is the superconducting gap) is dominated by the imaginary part of the conductivity, which, at finite temperature, is much greater than the real part in magnitude and is strongly frequency dependent ($\sigma = \sigma_1 - i\,\sigma_2,\ \sigma_2 \sim 1/\omega$). However, at THz frequencies ($>2\Delta/\hbar$), the real part of the conductivity plays also a role even at distances from the boundary larger than λ_L. Here we replace ϵ with the effective ϵ_{xx} given by the MM SPP:

$$\epsilon_{xx}(\omega) = \frac{\pi^2 d^2\,\epsilon_g}{8a^2}\left(1 - \frac{\pi^2 c^2}{\omega^2 a^2\,n_g^2}\right),$$
$$\omega_{\rm spp}^2 = \frac{\pi^2 c^2}{a^2\,n_g^2}, \tag{13}$$

where ϵ_g and n_g are the dielectric constant and refraction index of the material in the holes [17]. $\omega_{\rm spp}$ is assumed to be rather independent of k_x in the range where the dispersion has reached saturation. In this approximation, the motion equation for the electric field at the boundary is

$$-\omega^2 E + \omega_{\rm spp}^2 E = -\omega^2\,\rho(\omega)\,J(k_x,\omega). \tag{14}$$

The system of Eqs. (11) and (14) provides the eigenvalues which are solution of

$$\omega^4 - \omega^2\left(\omega_{\rm spp}^2 + \omega_{pJ}^2 + i\,\frac{\omega\,c^2}{4\pi\,\lambda_L^2}\,\rho(\omega)\right) + \omega_{\rm spp}^2\omega_{pJ}^2 = 0.$$

The anticrossing which arises from this very crude approach appears in Fig. 4. The dissipated power can be extracted by squaring Eq. (14) and by using $\rho(\omega) = \{-i\omega[\epsilon_{xx}(\omega) - 1]\}^{-1}$:

$$-i\,\omega|E|^2 \propto \frac{1}{\left(1 - \frac{\omega_{\rm spp}^2(k_x)}{\omega^2}\right)^2}\frac{1}{[\epsilon_{xx}(\omega) - 1]^2}\,\rho(\omega)|J|^2 \tag{15}$$

and has been plotted in Fig. 5 as a function of ω. It is peaked at the crossing point $k_x d/\pi \sim 0.6$. Equations (11) and (14) are coupled to the equation of motion of the fluxon [Eq. (4)]

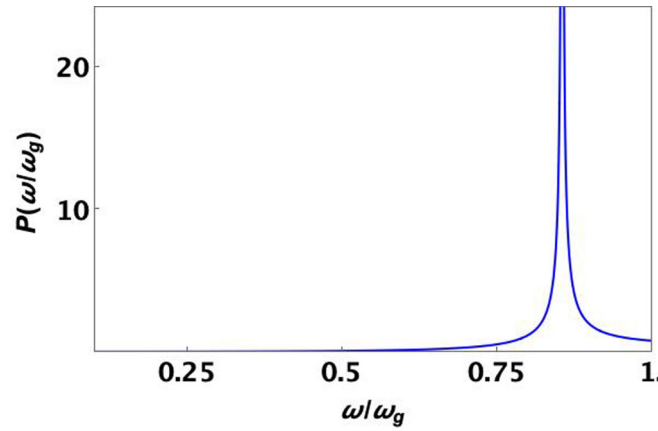

FIG. 5. Dissipated power at the anticrossing at the mode interaction vs ω, from Eq. (15). The parameters are the same as in Fig. 3.

because the propagation velocity u is required to define the dispersion of the radiating field generated by the fluxon [Eq. (8)]. Forcing terms acting in the superconducting phase dynamics arising from $B_y^{\rm source}$, the magnetic field generated by the TEM incoming wave, are derived in the next section.

V. THE FLUXON MOTION EQUATION IN THE PRESENCE OF RADIATION

The goal of this section is to extend the S-G equation [Eq. (4)] to include the presence of the SPP perturbation and the induced radiating fields. Indeed, the modulation in the top contact due to the presence of the grooves is responsible for extra radiation by the fluxon during its dynamics. Special concern, in the presence of radiating fields, is for the dissipation mechanisms in the junction. Both effects generate a current imbalance at the interface $J_+ - J_-$, and an added extra field $B^{(2)}$. Extension of Eq. (3) implies that two extra terms have to appear in Eq. (3): curl $B^{(2)}$ in the first term on the left-hand side (l.h.s.) of Eq. (3) and the imbalance current $J_+ - J_-$ on the right-hand side (r.h.s.) of Eq. (3). They will account both for the SPP generated by the incoming radiation and for the radiating fluxon itself. As discussed in Appendix C, Eq. (2) has to be rewritten as [Eq. (C6)]

$$\frac{\phi_0}{2\pi}\,\frac{\partial\varphi}{\partial x} = \frac{4\pi\lambda_L^2}{c}[J_+ - J_-] - (2\lambda_L + d_i)\,B_y - \lambda_p\,B_y^{(2)}. \tag{16}$$

The penetration length λ_p is discussed here below.

In Appendix C we derive an expression for curl $B^{(2)}$ which contributes to the motion equation of Eq. (4) with a dissipative term, the usually called β term [see Eq. (21) given here below]. Finally, using the London equation [see Appendix C, Eq. (C7)] we obtain [42]

$$\nabla\times\nabla\times\vec{B}^{(2)}\Big|_y + \frac{1}{\lambda_\omega^2}\,B_y^{(2)} = -\frac{4\pi}{c}\,\frac{\hbar}{2e\,d}\,\sigma_{qp}\frac{\partial^2\varphi}{\partial t\,\partial x}, \tag{17}$$

$$\text{with}\quad \frac{1}{\lambda_\omega^2} \equiv \frac{1}{\lambda_L^2} + \epsilon_b(\omega)\frac{\omega^2}{c^2} \tag{18}$$

$$\text{and}\quad \epsilon_b(\omega) = \epsilon_b + \frac{4\pi\,i\,\sigma_b}{c^2\,\omega}.$$

Equation (18) can be interpreted as follows. $2\pi/\lambda_\omega$ plays the role of k_x. By choosing $\epsilon_b \sim 41.4$ (Nb in the THz range $\omega \sim \pi \times 10^{13}$ Hz), we get $\lambda_\omega^{-1} \sim 2.1 \times 10^6$ m$^{-1} = k_x/2\pi$ ($\lambda_L \sim 50$ nm). On the other hand,

$$-ik_z = \sqrt{k_x^2 - \omega^2/c^2} \sim \frac{\pi}{d}\sqrt{(0.63)^2 - \left(\frac{0.8}{2}\frac{d}{h}\right)^2} \sim 4.4 \times 10^6 \text{ m}^{-1}. \quad (19)$$

k_z is purely imaginary and provides the decay of the $B^{(2)}$ field within the top superconducting contact. We define the inverse of $|k_z|$ as the penetration depth λ_p of the field ~230 nm.

Equation (17) with the definition of λ_ω of Eq. (18) are the starting point of our analysis. With an exponentially decaying dependence on the z coordinate, e^{-z/λ_p} of all the fields involved within the overlap junction region we can introduce an effective 1D Green function $G(x, x', \omega)$, with zero boundary conditions at $x = 0$ and $x = L$. $G(x, x', \omega)$ inverts the differential operator in Eq. (17) with $ik = [1/\lambda_\omega^2 - 1/\lambda_p^2]^{1/2}$ (k real):

$$[\vec{\nabla}^2 - k^2]\, G(x, x', \omega) = -\delta(x - x'). \quad (20)$$

Hence, $\nabla_x B_y^{(2)}(x,t) = \nabla \times \vec{B}^{(2)}|_z$ solves the integral equation

$$\nabla_x B_y^{(2)}(x,t) = \nabla_x B_y^{\text{source}}(x,t) - \frac{1}{\lambda_L^2}\int dx'\, dt'\, \nabla_x\, G(x, x', t-t')\, \mathcal{F}[\varphi(x', t')], \quad (21)$$

where

$$\mathcal{F}[\varphi(x,t)] = \frac{2\,\phi_o\,\lambda_L^2}{d\,c^2}\,\sigma_{qp}\,\frac{\partial^2\varphi}{\partial t\,\partial x} \quad (22)$$

and we have also added the contribution of B_y^{source} as an inhomogeneous term to be included in Eq. (3). Deriving Eq. (16) with respect to x, we insert $\nabla_x B_y^{(2)}(x,t)$ from Eq. (21) in it and divide the resulting equation by J_c/c. The extended form of Eq. (4), which includes a β-dissipative term, is obtained:

$$\lambda_J^2\frac{\partial^2\varphi}{\partial x^2} - \frac{1}{\omega_J^2}\frac{\partial^2\varphi}{\partial t^2} - \alpha\,\frac{1}{\omega_J}\frac{\partial\varphi}{\partial t} + \beta\int dt'\int dx'dz'\, G(x, x', t-t')\,\frac{\partial^3\varphi}{\partial t\,\partial x\,\partial x} - \sin[\varphi(x,t)] + \gamma$$
$$= \frac{8\pi^2\lambda_L^2}{\phi_0 c}\nabla_x[J_+ - J_-] + \frac{\lambda_p}{d_i + 2\lambda_L}\frac{c}{J_c}\nabla_x B_y^{\text{source}}(x,t),$$
$$\alpha = \frac{\hbar\omega_J}{2eRI_C}, \quad \beta = \sigma_{\text{qp}}\,\frac{2\phi_0\,\omega_J}{J_c\,c\,d_i}, \quad \phi_0 = hc/2e, \quad \gamma = \frac{J_{\text{ext}}}{J_c}. \quad (23)$$

We have integrated the integral of Eq. (21) by parts. The term at the boundary vanishes due to the chosen boundary conditions, so that the β term displays the third order derivative of the field φ. A current source term γ has also been included.

Usually no retardation is assumed in Eq. (23), so that $G(x, x', \omega) \sim G_k(x, x')$. The Green's function could account for the periodicity of the grooves potential following the lines of Ref. [35] but, as $\lambda_J \gg d$, we can expect that the modulation of the potential is on a much smaller scale than the scale characterizing the fluxon dissipation so that we can treat the superconductor MM as an effective homogeneous medium. This is consistent with a similar approximation which gives rise to the SPP dispersion. Moreover, it is customary to turn to a local approximation for the kernel, so that the integral in Eq. (23) disappears. Then, the motion equation for the phase driven by the plasmonic magnetic field B_y^{source}, in dimensionless coordinates $t \to \omega_J t$ and $x \to x/\lambda_J$, takes the usual form (see below):

$$\varphi_{xx} - \varphi_{tt} - \sin\varphi = \alpha\,\varphi_t - \beta\,\varphi_{xxt} - \gamma - g(t,x), \quad (24)$$

where $g(t,x)$ includes the forcing terms, on the r.h.s. of Eq. (23).

We concentrate now on the two added terms included in $g(t,x)$, produced by the SPP. From Eq. (11), the Fourier transform of the current difference term gives

$$-\frac{4\pi\lambda_L^2}{c}[J_+ - J_-] = i\,\frac{\omega}{\omega^2 - \omega_{pJ}^2}\,c\,\delta E_x, \quad (25)$$

where δE_x is the difference in electric field component between the upper and lower boundary of the junction. Similarly, from $\vec{k}\times\vec{E} = \vec{B}\,\omega/c$, the last term reads

$$-\lambda_p\,B_y^{\text{source}} = -i\,\frac{c|k_z|\lambda_p}{\omega}\,\delta E_x, \quad (26)$$

where $-i\,k_z = \sqrt{k_x^2 - (\omega/c)^2} > 0$ (here ω is the frequency of the source radiation). We get

$$g(\omega, x) = -i\frac{2e\lambda_J^2}{\hbar\omega_J}\left[\frac{\omega}{\omega^2 - \omega_{pJ}^2} - |k_z|\lambda_p\frac{4\pi}{\omega}\right]\nabla_x\delta E_x(x). \quad (27)$$

At $\omega \approx \omega_{\text{spp}}$ the charge density modulation induced by the SPP, ρ_{spp}, appears as $\frac{\partial}{\partial x}\delta E_x^{\text{spp}}(x) = 4\pi\,\rho_{\text{spp}}(x)$. Here $Q_{\text{spp}} \equiv \lambda_p w L\,\rho_{\text{spp}}$ is defined as the charge imbalance induced by the oscillating SPP. We average over the length λ_J in the $\hat{x}$ direction, assuming an oscillating dependence e^{ikx} and in the transverse directions of cross-section $\lambda_p w$. We rewrite Eq. (27) in terms of the amount of charge Q_{spp}, singling out just one frequency $\omega \approx \omega_{\text{spp}}$:

$$g(\omega, x, t) \sim \frac{4\pi}{\hbar\omega_J}\,\frac{\omega}{\omega^2 - \omega_{pJ}^2}\,\frac{\lambda_J}{w}\,\frac{\sin k\lambda_J}{kL}\,\frac{e\,Q_{\text{spp}}}{\lambda_p}\cos\omega t. \quad (28)$$

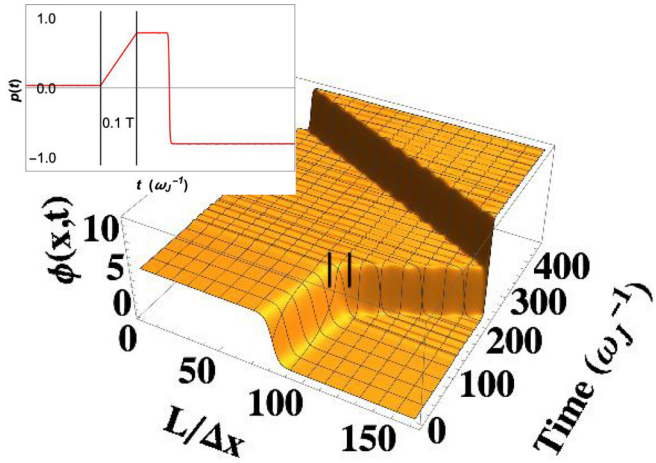

FIG. 6. 3D plot of the fluxon amplitude ϕ vs x and t. The initial velocity is $u/\bar{c} = 0.1$, far from resonance. A square pulse of small amplitude ($A = -0.1$, see text) acts between times 187 and 220 (duration 0.1 T), marked by the black slashes. The fluxon is sped up by the pulse. The inset shows the impulse of the field $P(t)$ vs t according to Eq. (29). The pulse acts in the time interval marked by the black lines.

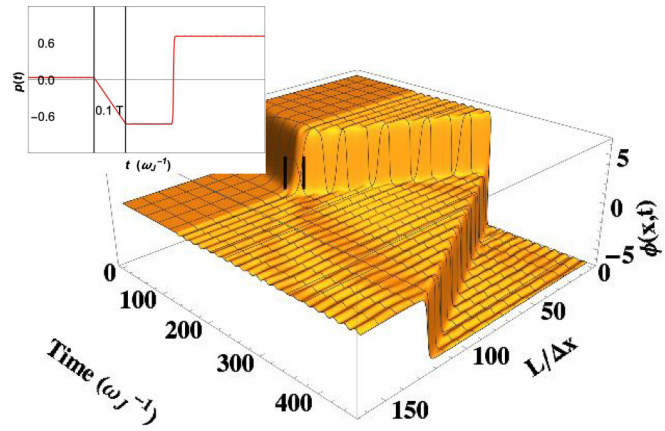

FIG. 7. 3D plot of the fluxon amplitude ϕ vs x and t. The initial velocity is $u/\bar{c} = 0.1$, same as Fig. 6. The amplitude of the square pulse is $A = 0.1$. The fluxon is scattered backward by the pulse. The inset shows the impulse of the field $P(t)$ vs t.

The largest contribution to the perturbation comes from the first term of Eq. (27), at frequency $\omega \approx \omega_{\rm spp} \approx \omega_{pJ}$. When the fluxon velocity provides a k_{pJ} close to the point at which the two dispersions cross [see Eq. (9)], the perturbation enters a resonance with the excitation modes of the combined system and its effect is largest. According to our parameters and to Fig. 3, this occurs at velocity $u = 0.6\bar{c}$ which corresponds to $k_{pJ}d/\pi \sim 0.7$.

VI. DISSIPATIONLESS SIMULATED DYNAMICS OF THE PERTURBED FLUXON

Let us now consider a dissipationless dynamics of the fluxon perturbed at some given time $t_0 > 0$ by a short square pulse, acting for a restricted time interval ∼0.1 T. The effect of the perturbation depends on the incoming velocity of the fluxon, and, of course, on the perturbation strength. Depending on its sign, the perturbation can increase or decrease the propagation velocity of the traveling fluxon, and can even scatter back the fluxon. The sequence of figures (Figs. 6–14) shows the three-dimensional (3D) plots of the simulated dynamics of the fluxon $\varphi(x,t)$ vs x and t, in units λ_J and ω_J. The maximum displayed time in these plots is $T = 450\omega_J^{-1}$, while the length of the junction is $L \sim 25\,\lambda_J$. In the time interval $\Delta t \in (187, 220) \sim 0.1$ T a square pulse of the form $A\cos\omega_{pJ}t$, of amplitude A, is turned on, with $\omega_{pJ}/\omega_J = 0.33 \times 10^3$. The first sequence of plots (Figs. 6–9) monitors the propagation of a fluxon of incoming velocity $u/\bar{c} = 0.1$. For $A = \pm 0.1$ the fluxon is just sped up (Fig. 6) or slowed down till to velocity inversion (Fig. 7), respectively. The insets show the change in impulse $P(t, A)$ as a function of time:

$$P(t;A) \propto \int_0^L dx\, \varphi_t(x,t;A)\varphi_x(x,t;A), \qquad (29)$$

with a flip of the sign when the fluxon hits the junction edge and is reflected. During the time of the pulse the impulse increases approximately linearly and stabilizes at a higher value, when the perturbation is turned off. From the pulse switch off time, onward, some beating can be seen in the fluxon amplitude time dependence, which is left over by the perturbation. The fluxon is reflected when it reaches $x = L = 160$, as seen from the change of slope of the field and from the sudden change of sign of the impulse in the inset. Since then, the motion is again at constant impulse, but backwards. At the reflection, the amplitude of the fluxon jumps by 2π.

It is noticeable that the various scatterings induced by the pulse, with coexistence of forward and backward propagating waves, end up in an impulse which is strictly periodic with the dwelling of the superconducting phase excitation inside the Josephson junction. This is due to the fact that dissipative terms have not been included in the dynamics. The overshooting at each reflection is clearly seen.

By increasing the amplitude A of the forcing term, there is no qualitative change in the time evolution of the fluxon, till A reaches the value $A \sim 0.6$ (Fig. 8). Subharmonic oscillations and beating markedly increase but the amplitude of the kink is still limited to the 2π flux jump. Beatings appear as a consequence of screening of the incoming kink by the collection of scattered antikinks as it happens when an electric charged particle is screened by a bath of opposite charges. This is the classical analog of Friedel oscillations appearing in quantum scattering.

Figure 9 shows the φ evolution for $A = 0.62$. The pulse acts as a strong scattering potential, so that there are scattered components of the original fluxon which move backward and forward with different velocities, generated by the pulse itself which are reflected at the boundary $x = 0, L$. The various components of the field interfere heavily and the fluxon kink is fully lost. Even when the effect of the pulse is over, such an interference generates an overshooting in the impulse at the reflection at the boundary, which is reabsorbed in a finite time in the multiple interference processes (see inset). Again, the inset shows the impulse of the system as a function of

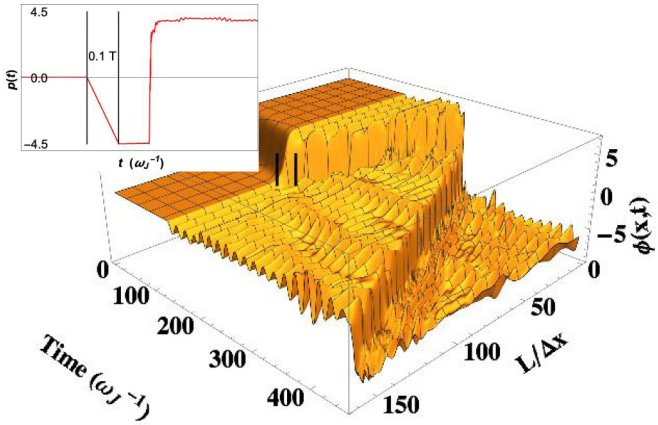

FIG. 8. 3D plot of the fluxon amplitude ϕ vs x and t, same as Fig. 6, for initial velocity $u/\bar{c} = 0.1$ and $A = 0.6$. The fluxon is sped up, but its shape is conserved except for beatings which mark the approach of a critical perturbation. The inset shows the impulse of the field $P(t)$ vs t.

time. However, it is a space integrated quantity, so that it captures only the average of the complex evolution. During the overshooting time and beyond, the phase field rolls down to higher and higher values, as confirmed by the voltage difference at the junction integrated over the whole junction length:

$$V(t;A) \propto \int_0^L dx\, \varphi_t(x,t;A), \tag{30}$$

which is plotted in Fig. 10 for $A = 0.8$. Of course the physical phase difference amplitude is mod$[2\pi]$. While the shape of the kink is lost, the propagation across the junction with reflection at the edges survives and strongly characterizes the impulse for larger evolution in time. This is reported in Fig. 11 for $A = 0.8$ (*red curve for* $u/\bar{c} = 0.1$).

The sequence Figs. 12–14 corresponds to the sequence Figs. 6–9 but for $u/\bar{c} = 0.6$, which implies that the k_x vector

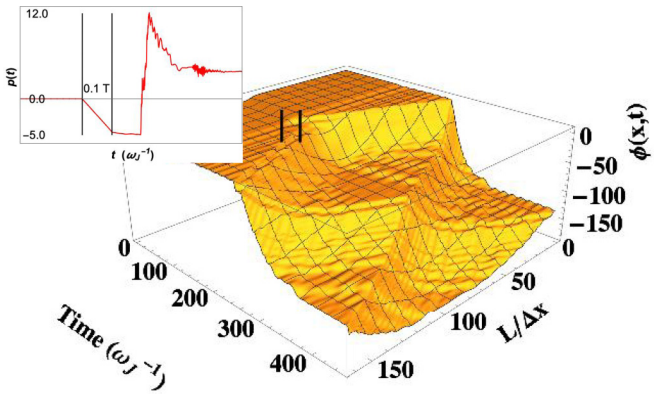

FIG. 9. 3D plot of the fluxon amplitude ϕ vs x and t, same as Fig. 6, for initial velocity $u/\bar{c} = 0.1$ and $A = 0.62$. The perturbation scatters the fluxon both backwards and forwards. The various components of the field interfere heavily and the fluxon itself is lost, while acquiring and eventually losing extra impulse (see inset). The phase difference rolls down with time when the effect of the pulse (but not the acquired impulse) is over.

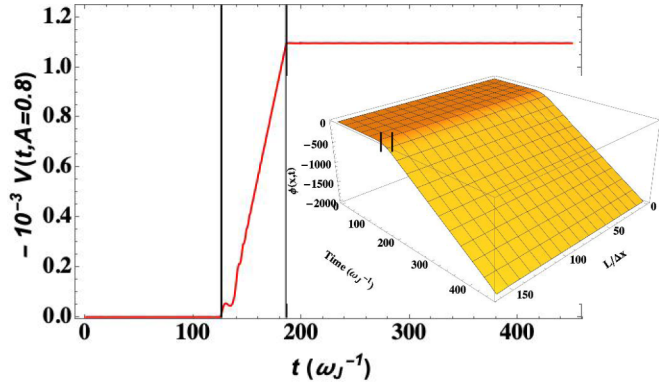

FIG. 10. Integrated voltage in units $\hbar\omega_J/2e$ vs t for initial velocity $u/\bar{c} = 0.1$ and $A = 0.8$ [see Eq. (30)]. The phase ϕ vs x and t rolls down almost uniformly in time for any x as shown in the 3D-plot inset.The pulse acts in the time interval marked by the black lines.

is close to the point where anticrossing occurs in Fig. 4. We made the choice of keeping similar strength of the perturbation A, although, according to Eq. (28), there would be an extra factor of $\sim$20 included in A in this case, to account for the vicinity to the pole. Apart for the obvious increase of the strength of the perturbation due to this extra factor, two features can be noticed when the initial velocity of the fluxon increases. Comparing Fig. 8 with Fig. 13 with the same perturbation strength A, the evolution of the fluxon having an initial velocity $u/\bar{c} = 0.6$ appears to be less sensitive to beating and subharmonic oscillations than when the fluxon is moving slower. On the other hand, the overshooting of the impulse when the fluxon inverts its motion at the edges is even larger as shown in Fig. 11. This corresponds to a faster roll down of the phase as marked by the larger scale for φ, which appears in Fig. 14, when compared to Fig. 8.

Let us now inquire up to what SPP charge $\tilde{Q}_{\rm spp}$, the fluxon may be assumed to be insensitive to the pulse. In other words, to which extent the forcing term can simply neutralize some

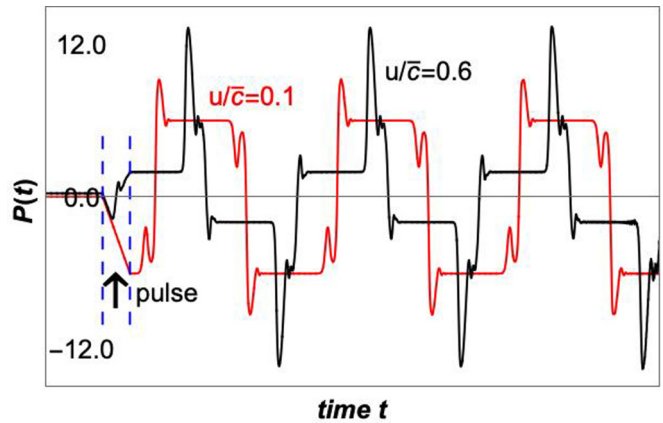

FIG. 11. Long time comparison of impulse $P(t)$ vs t at perturbation amplitude $A = 0.8$ between $u/\bar{c} = 0.1$ and $u/\bar{c} = 0.6$. The periodicity arises from reflection at the boundaries. The step of the timescale has been adjusted to present graphically comparable periods for the two velocities. The arrow points at the time interval during which the square pulse is active.

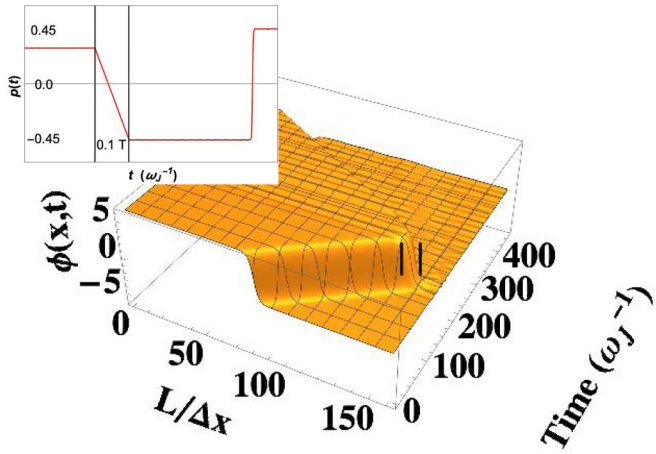

FIG. 12. 3D plot of the fluxon amplitude ϕ vs x and t. The initial velocity is $u/\bar{c} = 0.6$, which locates the k vector close to the resonance, according to Eq. (9). A square pulse of small amplitude $A = 0.1$, acts between times 187 and 220 (duration 0.1 T), marked by the black slashes. The fluxon is backscattered by the pulse. The inset shows the impulse of the field $P(t)$ vs t according to Eq. (29). The pulse acts in the time interval marked by the black lines.

dissipation induced by a term $-\alpha\varphi_t$ appearing in the motion equation. Let $\tilde{T}$ be the timescale of the SPP pulse. Qualitatively, ignoring the β term which is expected to be small, we can estimate a compensation on the average, between the forcing term and the dissipative α term:

$$-\alpha \int_{-L/2}^{+L/2} dx \int_0^{\tilde{T}} dt\ \varphi_t\ e^{-t/\tilde{T}} \cos\omega_{pJ} t$$

$$= 8\pi^2 \rho_{\rm spp} \frac{w}{\phi_0} \int_{-L/2}^{+L/2} dx \int_0^{\tilde{T}} dt\ e^{-t/\tilde{T}} \cos^2\omega_{pJ} t,$$

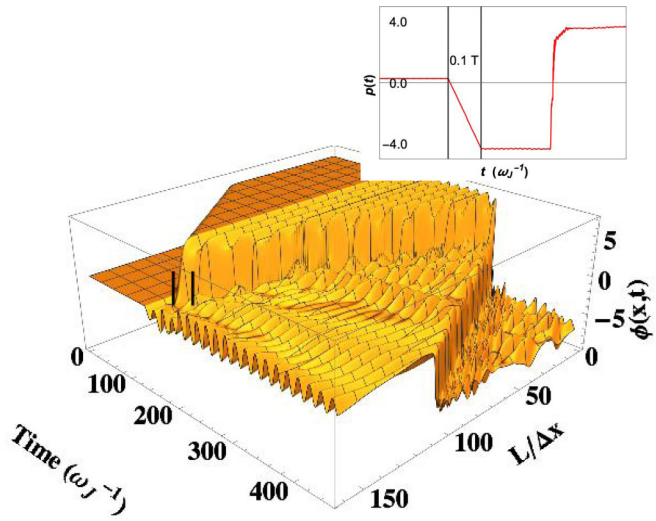

FIG. 13. 3D plot of the fluxon amplitude ϕ vs x and t. The initial velocity is $u/\bar{c} = 0.6$ (same as Fig. 12), with a pulse amplitude $A = 0.6$, close to the critical value. Heavy beating form but the fluxon shape can still be recognized. The inset shows the impulse of the field $P(t)$ vs t.

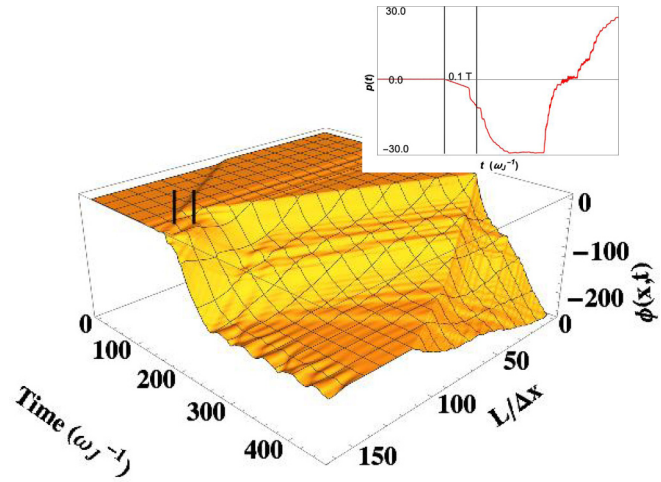

FIG. 14. 3D plot of the fluxon amplitude ϕ vs x and t, same as Fig. 6, for initial velocity $u/\bar{c} = 0.1$ and $A = 0.6$. The fluxon is sped up, but its shape is conserved except for beatings which mark the approach of a critical perturbation. The inset shows the impulse of the field $P(t)$ vs t.

i.e.,

$$2\pi\alpha \frac{u}{1+(\omega_{pJ}\tilde{T})^2} = \lambda_p L w\ \rho_{\rm spp} \frac{\lambda_J}{\lambda_p} \frac{1+2(\omega_{pJ}\tilde{T})^2}{1+4(\omega_{pJ}\tilde{T})^2}, \quad (31)$$

where the unperturbed fluxon waveform $\varphi(x-ut)$ of Eq. (6) has been used.

The requirement that $u < 1$ implies $(\omega_J\tilde{T} \ll 1 \ll \omega_{pJ}\tilde{T})$ that the overall induced charge by the SPP, $\tilde{Q}_{\rm spp} = \lambda_p L w\ \tilde{\rho}_{\rm spp}$, has to satisfy the inequality

$$\tilde{Q}_{\rm spp} < \frac{\alpha}{2\pi} \frac{\lambda_p}{\lambda_J} \frac{1}{(\omega_{pJ}\tilde{T})^2}, \quad (32)$$

which is quite a stringent condition on the intensity of the incoming radiation.

VII. CONCLUSIONS

Integrating superconductive and optical networks in a low temperature environment is becoming more and more desirable for quantum information processing, but it faces a longstanding problem. While optical fibers and optical circuits mostly involve frequencies in the infrared or, recently, THz frequency window, typical frequencies of a superconducting device are in the microwave range. On the other hand, the possibility of putting fluxons traveling in a long Josephson junction (JJ) in interaction with optical signals would increase enormously their flexibility as a tool for biasing and controlling gates in a classical or quantum circuit. Recently, optically generated spoof plasmon polaritons (SPPs) can be read out by means of integrated superconducting single-photon detectors [10] and, in general, interaction of a Josephson junction with a surface plasmon allows us to limit the power delivered to the junction and to avoid large increase of quasiparticle excitations. Still, optimization of energy exchange between a surface plasmon and a fluxon requires that the difference in frequency between the two-excitation modes is somehow reduced. We have shown that a feasible way to reach this

goal is to engineer one of the banks of the JJ in the form of a metamaterial (MM) which has been proved to generate a SPP at THz frequency [18], when irradiated with a source in the infrared. The SPP can be absorbed by the moving fluxon.

We have shown that the two excitation modes, SPP and fluxon radiative field, can interact (see Fig. 4). Indeed, the MM bank induces a radiative field by the fluxon of comparable frequency. The typical anticrossing in the dispersion is due to charge oscillations at the MM bank, which gives rise to absorption of impulse by the fluxon. The latter can be sped up or slowed down or even scattered backwards by interaction with a pulsed SPP, which acts as a forcing term on the Sine-Gordon (S-G) dynamics of the fluxon, driven by the oscillations of the SPP charge.

We provide examples of the simulated S-G dissipationless dynamics of a fluxon in a long JJ in which a free propagating fluxon is acted on by the SPP perturbation for a limited time interval. The boundary conditions for φ_x in the motion equation are standard [34]. We show that the fluxon field acquires subharmonic oscillations and beating, due to extra impulse absorbed from the perturbation, without losing its kink shape, unless the perturbation amplitude is higher than a critical value, which depends on the initial velocity, which is in the vicinity of the anticrossing point. Indeed, the fluxon keeps being rather robust but, meanwhile, it generates interference of extra 2π jumps. This happens because the soliton energy is two orders of magnitude larger than the energies of the excitation modes of Fig. 4, involved. For perturbation amplitudes higher than the critical value, the fluxon field loses its shape, but not the periodic dwelling motion, with reflections at the edge of the junction. The superconducting phase rolls down as in a washboard potential and a marked kink in the voltage appears (see Fig. 11). Increasing the initial velocity of the fluxon makes it more robust up to the critical perturbation strength, but lowers the threshold of criticality quite a lot, because the anticrossing point is approached.

We argue in Appendix B, with an approach similar to the standard one reported in Appendix A, that dissipative terms in the motion equation do not affect qualitatively the fluxon motion provided an applied current bias is fed in the junction. This is because the MM has a structure on a scale of hundreds of nanometers, much smaller than the typical length scale of the junction dynamics λ_J [43]. However, this also requires that the junction itself is quite long, up to millimeters.

In our idealized geometry, the SPP is generated by low power infrared radiation impinging on the top superconducting MM electrode. Of course challenging problems arise in the actual fabrication of the device which are left out of this paper. Crucial is the shielding to substantially reduce light induced quasiparticle excitations while, in the meantime, guaranteeing good matching between the impinging radiation and the radiation captured by the MM. Actually, infrared radiation is just below the threshold for quasiparticle excitation in bulky contacts out of, e.g., Nb nitride or Nb. On the other hand, thermal heating is limited by the the choice of isolated light pulses of picosecond duration, a time interval of the order of quasiparticle relaxation time [44].

ACKNOWLEDGMENTS

We acknowledge useful discussions with G. Filatrella, D. Giuliano, P. Lucignano, and G. Miano. This work was supported financially by University of Napoli "Federico II" with project PLASMJAC, E62F17000290005.

APPENDIX A: FLUXON ENERGY IN THE DISSIPATIONLESS CASE

Let us neglect for the time being the electromagnetic source in the motion equation for the fluxon, Eq. (24). The γ term accounts for a current source and can sustain the propagation of the fluxon along the junction compensating the dissipations. In the infinite length limit for the junction an energy eigenmode for the fluxon can be derived. When considering the motion equation, Eq. (23), the eigenmode will have a dispersion characterized by the k vector k_x. The 3D Hamiltonian H_0 for the fluxon in the absence of dissipation is

$$H_0 = \frac{\hbar}{2e} J_c \, \lambda_J^2 \int d\tilde{x} \left[\frac{1}{2} (\varphi_{\tilde{t}})^2 + \frac{1}{2} (\varphi_{\tilde{x}})^2 + (1 - \cos\varphi) \right],$$

with $\tilde{t} = \omega_J t$ and $\tilde{x} = x/\lambda_J$. We drop the tilde in the following, unless needed. We drop for the time being the prefactor in front of the integral which can also be rewritten as $\{\phi_o^2/[8\pi^2(2\lambda_L + d)]\} \times 1/2\pi$. In the infinite length limit for the junction, let us consider a forward moving fluxon of the form of Eq. (6). The energy of the soliton is easily calculated:

$$\mathcal{E}_0^{\rm sol} = \frac{8}{\sqrt{1-u^2}}, \tag{A1}$$

where u is the velocity in unity of the light velocity c, and is conserved:

$$\frac{\partial H_0}{\partial t} = \int dx \, \varphi_t [\varphi_{xx} - \varphi_{tt} - \sin\varphi] = 0. \tag{A2}$$

If we neglect the β term and we use the form of the dissipationless fluxon of Eq. (6), but with a perturbed steady state velocity of the fluxon driven by the current $J_{\rm ext}$ ($\gamma = J_{\rm ext}/J_c$):

$$\alpha \, \frac{8 \, u_\infty/\bar{c}}{\sqrt{1-(u_\infty/\bar{c})^2}} = 2\pi \, \gamma, \quad \left(\frac{u_\infty}{\bar{c}}\right)^2 = \frac{1}{1+\left(\frac{4\,\alpha}{\pi\,\gamma}\right)^2},$$

$$E_0^{\rm sol} = \frac{8}{\sqrt{1-(u_\infty/\bar{c})^2}} = \frac{2\pi\,\gamma\,\bar{c}}{\alpha\,u_\infty} = 8\sqrt{1+\left(\frac{\pi\,\gamma}{4\,\alpha}\right)^2}. \tag{A3}$$

These results are well known [32].

APPENDIX B: DISSIPATIVE TERMS IN THE ABSENCE OF EXCITATION MODES INTERACTION

In our approximations we expect that the dissipative terms, in the presence of a bias current γ, lead to a stationary state dynamics which is not qualitatively different from the dynamics presented in the dissipationless simulation of Sec. VI. The dissipation losses should be compensated by the driving current. In the absence of the forcing term, the fluxon velocity u can be determined following the same lines of Appendix A, with inclusion of the β term. In analogy with Eq. (A2), we

impose

$$\alpha\,\frac{1}{\omega_J}\int dx\,(\partial_t\varphi)^2-\beta\int dxdx'\left[\frac{\partial\varphi}{\partial t}(x,t)\,G[k(x,x')]\times\frac{\partial^3\varphi}{\partial t\partial^2x'}(x',t)\right]-\int dx\,\gamma\,\partial_t\varphi=0. \tag{B1}$$

As in the derivation of the SPP, we rely on the fact that the MM modulation is subwavelength and that all space dependencies are on a scale larger that the periodicity d of the groove lattice. In particular, $k=2\pi/\lambda_\omega\ll\pi/d$, so that we can consider just average homogeneous MM contacts and the Green's function $G(k;x,x')$ satisfying Eq. (20) and vanishing at the junction edge, takes the simple form

$$G(k;x,x')=\frac{1}{k\,\sinh kL}[\sinh k(L-x_>)\,\sinh kx_<], \tag{B2}$$

where $x_>$ ($x_<$) is the larger (smaller) argument between x,x'. Far from the edges, we can approximate the unperturbed kink $\varphi(\xi)$ as a step function at $\xi=x-ut=L/2$. Hence, φ_t has even symmetry in space with respect to $L/2$, while φ_{tx} has odd symmetry. On the other hand, $G(k;x,x')\sim G(k|x-x'|)$ and a double integration by parts changes the β term into

$$\int dxdx'\left[\frac{\partial\varphi}{\partial t}(x,t)\,\frac{\partial^2}{\partial x\partial x'}G(k;x,x')\,\frac{\partial\varphi}{\partial t}(x',t)\right]. \tag{B3}$$

Here $\frac{\partial^2}{\partial x\partial x'}G(k;x,x')$ is very localized at $x\sim x'$, so that this term can be changed into a local term which renormalizes the α term. The derivation of u_∞ given in Appendix A follows.

APPENDIX C: FORCING TERMS IN THE NONDISSIPATIVE S-G EQUATION OF MOTION

Let us now derive the forcing terms to be added in the S-G equation of motion Eq. (4), assumed to be one dimensional and nondissipative ($\alpha'=0$).

From Eq. (2), the phase jump between the two edges of the insulating layer is

$$\frac{\partial\vartheta_+}{\partial x}-\frac{\partial\vartheta_-}{\partial x}=\frac{8\pi^2\lambda_L^2}{\phi_o c}[J_+-J_-]-\frac{2e}{\hbar c}\,[A_x(+\infty)-A_x(-\infty)], \tag{C1}$$

$[J_+-J_-]$ is the difference of superconducting screening currents at the barrier boundaries of the Josephson junction. Equation (C1) is consistent with the London equation (C2b):

$$\frac{\partial J^s}{\partial t}=\frac{n_se^2}{m}\vec{E}\Big|_b,\qquad \nabla\times\vec{J}^s+\frac{n_se^2}{mc}\vec{B}=0. \tag{C2}$$

In fact, usually the contacts are bulk superconductors and the $\vec{A}$ field decays far from the edge on the scale of λ_L and it is possible to take a circuit with $z_\pm$ well within the bulk so that $J_\pm\equiv J(z_\pm)$ vanish and the circulation of $\vec{A}$ along the circuit provides the full flux piercing the weak link area $(2\lambda_L+d_i)LB_y$. In the limit to an inhomogeneous but spacially continuous superconductor, $2\lambda_L+d_i\to z_+-z_-\to 0$, a local expression can be obtained and the finite difference of the currents $J_\mp$ divided by z_+-z_- turns into the curl of the screening currents:

$$\frac{[J_--J_+]}{2\lambda_L+d_i}\to-\partial_zJ_x^{sb}\sim-\nabla\times\vec{J}^{sb}|_y \tag{C3}$$

(the label b stands for "bulk"). Similarly, for a continuous phase

$$-\frac{\frac{\partial\vartheta_+}{\partial x}-\frac{\partial\vartheta_-}{\partial x}}{2\lambda_L+d_i}\to\vec{\nabla}\times\vec{\nabla}\vartheta|_y=0. \tag{C4}$$

so that the $\hat{y}$ component of the London equation (2) is recovered [$1/\lambda_L^2=(4\pi n_se^2/mc)$]:

$$0=-\nabla\times\vec{J}^{sb}|_y-(n_se^2/mc)\,B_y|_b. \tag{C5}$$

However, there are two crucial differences in our case. On the one hand, the thickness of the superconducting contacts in the overlap junction is finite and relatively small. On the other hand, there is the SPP leaking into the upper superconducting edge generated by the MM at the top, which does not allow us to drop the difference in the current flowing between the two contacts. We assume that the perturbed phase difference φ depends on the current imbalance induced by the plasmon and on the source field $B_y^{\rm source}$, which penetrates a distance λ_p along the $\hat{z}$ direction (λ_p is discussed in the text). It follows that Eq. (C1), along the $\hat{x}$ direction, takes the form

$$\frac{\phi_0}{2\pi}\,\frac{\partial\varphi}{\partial x}=-(2\lambda_L+d_i)\,B_y+\frac{4\pi\lambda_L^2}{c}[J_+-J_-]_{\rm spp}-\lambda_p\,B_y^{\rm source}, \tag{C6}$$

where we assume that $B_y=B^{(1)}+B^{(2)}$, where $B^{(1)}$ is the one generated by the fluxon in the absence of the external source and $B^{(2)}$ is the one giving rise to radiating effects.

In the following we derive an expression for curl $B^{(2)}$, which contributes to the motion equation of Eq. (4) with a dissipative term, the usually called β term [see Eq. (21)]. We will drop the magnetic field generated by the Josephson current itself in the derivation, which is usually considered to be small. We have, excluding the term due to the source $B_y^{\rm source}$, for the time being

$$\begin{aligned}\nabla\times\nabla\times\vec{B^{(2)}}|_y&=\partial_z(\nabla\times\vec{B^{(2)}}|_x)-\partial_x(\nabla\times\vec{B^{(2)}}|_z)\\&=\frac{\partial}{\partial z}\left[\frac{4\pi}{c}J_x^b+\frac{4\pi\lambda_L^2}{c}\left(\frac{4\pi\,i\,\sigma_b\,\omega}{c^2}+\epsilon_\infty\frac{\omega^2}{c^2}\right)J_x^b\right]\\&\quad-\frac{\partial}{\partial x}\left[\frac{4\pi}{c}\,J_z|_T\right].\end{aligned} \tag{C7}$$

Here J_x^b denotes the superconducting screening currents induced by the radiation at the boundary of the contacts. The first square bracket term in the r.h.s. arises from the Maxwell-Ampere equation

$$\nabla\times\vec{B^{(2)}}|_x=\frac{4\pi}{c}J_x+\frac{1}{c}\frac{dD_x^{(b)}}{dt}, \tag{C8}$$

where the total current J also includes a contribution from the Ohmic transport, $J=J^b+J^{nb}=J^b+\sigma_b\,E_b^{(2)}$. $\vec{D}^{(b)}$ is the electric induction vector penetrating in the contacts. Both $E_{bx}^{(2)}$ and $D_x^{(b)}$ of Eq. (C8) can be related to J_x^b itself, by means of

the Fourier transform ($\partial_t \to -i\,\omega$) of the London equation, Eq. (10): $E_{bx}^{(2)} = -4\pi\lambda_L^2\, i\,\omega\, J_x^b/c^2$.

The second square bracket term in the r.h.s. of Eq. (C7) accounts for the normal quasiparticle tunneling current $\vec{J}_n|_T$, oriented along $\hat{z}$. Quasiparticles excited due to the high operating frequency ($\omega \gg \Delta/\hbar$) contribute dissipatively to the current. The quasiparticle current coexists with the Josephson current $J_c \sin\varphi$. $\sigma_{\rm qp}$ is the corresponding quasiparticle conductivity and this term can be expressed in terms of the derivatives of the phase difference φ:

$$\frac{4\pi}{c}\frac{\partial J_z^{nT}}{\partial x} = \frac{4\pi}{c}\sigma_{\rm qp}\frac{\partial E_z}{\partial x} \approx \frac{4\pi}{c}\frac{\sigma_{\rm qp}}{d}\frac{\partial V(z=0)}{\partial x} = \frac{4\pi}{c}\,\sigma_{\rm qp}\,\frac{\hbar}{2e\,d}\frac{\partial^2\varphi}{\partial t\,\partial x}.$$

Finally, according to Eq. (C5),

$$\left(\frac{4\pi}{c}\nabla\times J^{sb}\right)_y \approx \frac{4\pi}{c}\partial_z J_x^{sb} = -\frac{1}{\lambda_L^2}\,B_y^{(2)}, \tag{C9}$$

so that Eq. (C7) can be written as [42]

$$\nabla\times\nabla\times\vec{B}^{(2)}\Big|_y + \frac{1}{\lambda_\omega^2}\,B_y^{(2)} = -\frac{4\pi}{c}\,\frac{\hbar}{2e\,d}\,\sigma_{qp}\frac{\partial^2\varphi}{\partial t\,\partial x}, \tag{C10}$$

with $\dfrac{1}{\lambda_\omega^2} \equiv \dfrac{1}{\lambda_L^2} + \epsilon_b(\omega)\dfrac{\omega^2}{c^2}$

and $\epsilon(\omega) = \epsilon_\infty + \dfrac{4\pi\, i\,\sigma_b}{c^2\,\omega}$.

The full motion equation for the fluxon is reported in the text, Eq. (23).

[1] K. Heshami, D. G. England, P. C. Humphreys, P. J. Bustard, V. M. Acosta, J. Nunn, and B. J. Sussman, Quantum memories: Emerging applications and recent advances, J. Mod. Opt. **63**, 2005 (2016).

[2] R. Held, J. Xu, A. Schmehl, C. W. Schneider, J. Mannhart, and M. Beasley, Superconducting memory based on ferromagnetism, Appl. Phys. Lett. **89**, 163509 (2006).

[3] F. Giazotto, T. T. Heikkilä, G. P. Pepe, P. Helistö, A. Luukanen, and J. P. Pekola, Ultrasensitive proximity Josephson sensor with kinetic inductance read-out, Appl. Phys. Lett. **92**, 162507 (2008).

[4] R. McDermott, M. G. Vavilov, B. L. T. Plourde, F. K. Wilhelm, P. J. Liebermann, O. A. Mukhanov, and T. A. Ohki, Quantum-classical interface based on single flux quantum digital logic, Quantum Sci. Technol. **3**, 024004 (2018).

[5] A. I. Lvovsky, B. C. Sanders, and W. Tittel, Optical quantum memory, Nat. Photon. **3**, 706 (2009).

[6] F. Stella, M. Casalboni, M. Cirillo, V. Merlo, C. Palazzesi, G. P. Pepe, P. Prosposito, and M. Salvato, Integrating superconductive and optical circuits, Appl. Phys. Lett. **92**, 202505 (2008).

[7] T. I. Larkin, V. V. Bol'ginov, V. S. Stolyarov, V. V. Ryazanov, I. V. Vernik, S. K. Tolpygo, and O. A. MukhanovFerromagnetic Josephson switching device with high characteristic voltage, Appl. Phys. Lett. **100**, 222601 (2012).

[8] A. Politi, M. J. Cryan, J. G. Rarity, S. Yu, and J. L. O'Brien, Silica-on-silicon waveguide quantum circuits, Science **320**, 646 (2008).

[9] M. A. Jaspan, J. L. Habif, R. H. Hadfield, and S. W. Nam, Heralding of telecommunication photon pairs with a superconducting single photon detector, Appl. Phys. Lett. **89**, 031112 (2006).

[10] R. W. Heeres, L. P. Kouwenhoven, and V. Zwiller, Quantum interference in plasmonic circuits, Nat. Nanotechnol. **8**, 719 (2013).

[11] D. Sarid and W. Challener, *Modern Introduction to Surface Plasmons: Theory, Mathematical Modeling, and Applications* (Cambridge University Press, Cambridge, 2010).

[12] H. K. Hunta and A. M. Armani, Label-free biological and chemical sensors, Nanoscale **2**, 1544 (2010).

[13] E. Laux, C. Genet, T. Skauli, and T. W. Ebbesen, Plasmonic photon sorters for spectral and polarimetric imaging, Nat. Photon. **2**, 161 (2008).

[14] B. S. WilliamsTerahertz quantum-cascade lasers, Nat. Photon. **1**, 517 (2007).

[15] W. L. Barnes, A. Dereux, and T. W. Ebbesen, Surface plasmon subwavelength optics, Nature (London) **424**, 824 (2003).

[16] Z. Kang and G. P. Wang, Coupled metal gap waveguides as plasmonic wavelength sorters, Opt. Express **16**, 7680 (2008).

[17] J. B. Pendry, L. Martin-Moreno, and F. J. Garcia-Vidal, Mimicking surface plasmons with structured surfaces, Science **305**, 847 (2004).

[18] F. J. Garcia-Vidal, L. Martin-Moreno, and J. B. Pendry, Surfaces with holes in them: New plasmonic metamaterials, J. Opt. A **7**, S97 (2005).

[19] S. A. Maier, S. R. Andrews, L. Martin-Moreno, and F. Garcia-Vidal, Terahertz Surface Plasmon-Polariton Propagation and Focusing on Periodically Corrugated Metal Wires, Phys. Rev. Lett. **97**, 176805 (2006).

[20] C. Forestiere, G. Miano, G. Rubinacci, and L. Dal Negro, Role of aperiodic order in the spectral, localization, and scaling properties of plasmon modes for the design of nanoparticle arrays, Phys. Rev. B **79**, 085404 (2009).

[21] J. B. Pendry, A. J. Holden, W. J. Stewart, and I. Youngs, Extremely Low Frequency Plasmons in Metallic Mesostructures, Phys. Rev. Lett. **76**, 4773 (1996).

[22] L. Shen, X. Chen, and T.-J. Yang, Terahertz surface plasmon polaritons on periodically corrugated metal surfaces, Opt. Express **16**, 3326 (2008).

[23] C. Yeh, F. Shimabukuro, and P. H. Siegel, Low-loss terahertz ribbon waveguides, Appl. Opt. **44**, 5937 (2005).

[24] Y. J. Zhou and B. J. Yang, Planar spoof plasmonic ultra-wideband filter based on low-loss and compact terahertz waveguide corrugated with dumbbell grooves, Appl. Opt. **54**, 4529 (2015).

[25] P. Jung, A. V. Ustinov, and S. M. Anlage, Progress in superconducting metamaterials, Supercond. Sci. Technol. **27**, 073001 (2014).

[26] S. Butz, P. Jung, L. V. Filippenko, V. P. Koshelets, and A. V. Ustinov, A one-dimensional tunable magnetic metamaterial, Opt. Express **21**, 22540 (2013).

[27] J. Gu, R. Singh, Z. Tian, W. Cao, Q. Xing, M. He, J. W. Zhang, J. Han, H.-T. Chen, and W. Zhang, Terahertz superconductor metamaterial, Appl. Phys. Lett. **97**, 071102 (2010).

[28] S. Oh, D. Youm, and M. Beasley, A superconductive magnetoresistive memory element using controlled exchange interaction, Appl. Phys. Lett. **71**, 2376 (1997).

[29] M. Trepanier, D. Zhang, O. Mukhanov, and S. M. Anlage, Realization and Modeling of Metamaterials Made of rf Superconducting Quantum-Interference Devices, Phys. Rev. X **3**, 041029 (2013).

[30] N. Lazarides and G. P. Tsironis, rf superconducting quantum interference device metamaterials, Appl. Phys. Lett. **90**, 163501 (2007).

[31] D. Zhang, M. Trepanier, O. Mukhanov, and S. M. Anlage, Tunable Broadband Transparency of Macroscopic Quantum Superconducting Metamaterials, Phys. Rev. X **5**, 041045 (2015).

[32] M. Salerno, M. R. Samuelsen, G. Filatrella, S. Pagano, and R. D. Parmentier, Microwave phase locking of Josephson-junction fluxon oscillators, Phys. Rev. B **41**, 6641 (1990).

[33] M. Tinkham, *Introduction to Superconductivity* (McGraw-Hill International Editions, New York, 1996).

[34] P. S. Lomdahl, O. H. Soerensen, and P. L. Christiansen, Soliton excitations in Josephson tunnel junctions, Phys. Rev. B **25**, 5737 (1982).

[35] A. A. Golubov, I. L. Serpuchenko and A. V. Ustinov, Dynamics of a Josephson fluxon in a long junction with inhomogeneities: theory and experiment, Zh. Eksp. Teor. Fiz. **94**, 297 (1988) [Sov. Phys. JETP **67**, 1256 (1988)].

[36] G. Filatrella, B. A. Malomed, and R. D. Parmentier, Inverse ac Josephson effect for a fluxon in a long modulated junction, Phys. Lett. A **198**, 43 (1995).

[37] P. Salén, M. Basini, S. Bonetti *et al.*, Matter manipulation with extreme terahertz light: Progress in the enabling THz technology, Phys. Rep. **836**, 1 (2019),

[38] D. Montemurro, D. Massarotti, P. Lucignano, S. Roddaro, D. Stornaiuolo, D. Ercolani, L. Sorba, A. Tagliacozzo, F. Beltram, and F. Tafuri, Towards a hybrid high critical temperature superconductor junction with a semiconducting InAs nanowire barrier, J. Supercond. Novel Magn. **28**, 3429 (2015).

[39] D. Montemurro, D. Stornaiuolo, D. Massarotti, D. Ercolani, L. Sorba, F. Beltram, F. Tafuri, and S. Roddaro, Suspended InAs nanowire Josephson junctions assembled via dielectrophoresis, Nanotechnology **26**, 385302 (2015).

[40] G. N. Gol'tsman, K. Smirnov, P. Kouminov, B. Voronov, N. Kaurova, V. Drakinsky, J. Zhang, A. Verevkin, and R. Sobolewski, Fabrication of nanostructured superconducting single-photon detectors, IEEE Trans. Appl. Supercond. **13**, 192 (2003).

[41] G. S. Mkrtchyan and V. V. Shmidt, On the radiation from inhomogeneous Josephson junction, Solid State Commun. **30**, 783 (1979).

[42] L. N. Bulaevskii and A. E. Koshelev, Radiation from a Single Josephson Junction into Free Space Due to Josephson Oscillations, Phys. Rev. Lett. **97**, 267001 (2006).

[43] M. Taguchi, D. M. Basko, and F. W. J. Hekking, Mode engineering with a one-dimensional superconducting metamaterial, Phys. Rew. B **92**, 024507 (2015).

[44] P. J. de Visser, J. J. A. Baselmans, J. Bueno, N. Llombart, and T. M. Klapwijk, Fluctuations in the electron system of a superconductor exposed to a photon flux?, Nat. Commun. **5**, 3130 (2014).